Decoupling of translational and rotational diffusion in quasi-2D colloidal fluids

Skanda Vivek, and Eric R. Weeks

Citation: The Journal of Chemical Physics **147**, 134502 (2017); doi: 10.1063/1.4996733
View online: http://dx.doi.org/10.1063/1.4996733
View Table of Contents: http://aip.scitation.org/toc/jcp/147/13
Published by the American Institute of Physics

Decoupling of translational and rotational diffusion in quasi-2D colloidal fluids

Skanda Vivek[1,a)] and Eric R. Weeks[2]
[1]*Department of Physics, Georgia Institute of Technology, Atlanta, Georgia 30332, USA*
[2]*Department of Physics, Emory University, Atlanta, Georgia 30322, USA*

(Received 18 July 2017; accepted 13 September 2017; published online 3 October 2017)

We observe the translational and rotational diffusion of dimer tracer particles in quasi-2D colloidal samples. The dimers are in dense samples of two different sizes of spherical colloidal particles, with the area fraction ϕ of the particles varying from dilute to nearly glassy. At low ϕ, rotational and translational diffusion have a ratio set by the dimer size, as expected. At higher ϕ, dimers become caged by their neighboring particles, and both rotational and translational diffusion become slow. For short dimers, we observe rapid reorientations so that the rotational diffusion is faster than the translational diffusion: the two modes of diffusion are decoupled and have different ϕ dependence. Longer dimers do not exhibit fast rotations, and we find that their translational and rotational diffusion stay coupled for all ϕ. Our results bridge prior results that used spheres (very fast rotation) and long ellipsoids (very slow rotation). *Published by AIP Publishing.* https://doi.org/10.1063/1.4996733

I. INTRODUCTION

A comprehensive explanation for the dramatic increase in viscosity on approaching the glass transition is still lacking, although there are a variety of theories.[1–3] What makes the matter more complicated is the inadequacy of the traditional concept of viscosity and its relation with microscopic diffusion in supercooled liquids. In liquids, the Stokes-Einstein-Sutherland equation[4,5] relates microscopic translational diffusion (D_T) as inversely proportional to solvent viscosity η. Rotational diffusion (D_R) is also inversely proportional to η, known as the Stokes-Einstein-Debye relation. Further, the ratio of translational to rotational diffusion constants (D_T/D_R) should be independent of viscosity and temperature. However, many experiments and simulations[6–9] have shown a violation of the Stokes-Einstein and Stokes-Einstein-Debye relations in supercooled liquids. These violations can manifest as D_T and/or D_R no longer being inversely related to η and also D_T/D_R no longer being a constant.

Pioneering experiments in the early 1990s observed a violation of these relations on approaching the glass transition in orthoterphenyl.[6,7] Rotational and translational diffusion constants were measured indirectly through spin relaxations. They observed an enhancement of translation relative to rotation approaching the glass transition. At that time, this strange difference was attributed to the spatial distribution of relaxation time scales $\rho(\tau)$, and it measured rotation and translation measurements being sensitive to different moments of this distribution.[10] But it was thought that on the single molecule scale, translation and rotation remain coupled.

However, recent simulations and colloidal experiments have found that decoupling occurs even at the single particle level.[11–14] The current hypothesis is that decoupling occurs due to translation and rotation degrees encountering different dynamic length scales.[2] Moreover, some studies found that translation was enhanced relative to rotation,[14–16] whereas others found rotation was enhanced relative to translation.[11–13] These different experiments had different probe shapes and conditions so direct comparison of the observations is challenging.

In this study, we examine how the probe details influence translational-rotational decoupling in colloidal samples. Colloidal samples at high concentrations have been established as model glass formers[17,18] and have the advantage that individual particles can be visualized. Here we use naturally occurring anisotropic silica dimers of different aspect ratios as tracers and find that the dimer length determines translation-rotation decoupling.

These dimers are at a very low concentration, less than 5%, and the experiments are the same as previously published (where we studied only the monomer particles[19]). We find that for dimers of smaller lengths, rotations do not slow down as much as translations, on approaching the glass transition, similar to the case of spheres as probes.[13] However we find that in our longest dimers, D_T and D_R remain coupled at all concentrations, i.e., $D_T/D_R \sim$ constant. Figure 1 shows an example of computer rendering of a long dimer and short dimer in one of our samples. Our key result is that the shorter dimer can rotate more easily as it is easier to relax the steric hindrance of the neighboring particles.

II. MATERIALS AND METHODS

A. Experimental methods

For this work, we reanalyze movies corresponding to previously published data.[19] In the experiments, we use gravity to confine bidisperse non-functionalized silica particles to a monolayer (diameters $\sigma_S = 2.53$ and $\sigma_L = 3.38$ μm, Bangs Laboratories, SS05N). The number ratio is $N_L/N_S = 1.3 \pm 0.5$ and varies from sample to sample. The control parameter is the

a)Electronic mail: skanda.vivek@gmail.com

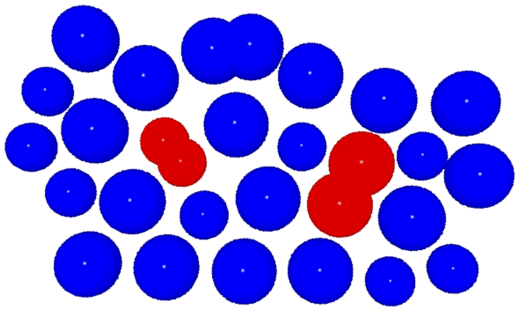

FIG. 1. Example of a short dimer ($l_l = 3.92\,\mu$m) and long dimer ($l_l = 5.37\,\mu$m) in a concentrated sample with area fraction $\phi = 0.79$. The rendering is adapted from particle positions. Dimers are in red, and neighbors are in blue. We find that short dimers can rotate more easily, whereas long dimers are more constrained by their neighbors.

area fraction ϕ, with glassy samples found for $\phi > 0.79$; the data we present here are all with $\phi < 0.79$. The particles are sedimented to the microscope coverslip of our sample chamber prior to observation. The coverslip is made hydrophobic by treatment with Alfa Aesar Glassclad 18 to prevent particle adhesion, and indeed we do not observe any particles stuck to the glass. We do not add salt. We verify that in all experiments, only one layer of particles is present (ensured by keeping the overall particle concentration below the level that requires a second layer to form). We use brightfield microscopy and a CCD camera to record movies of particles diffusing.

The samples have naturally occurring dimers at dilute concentrations from 2% to 5%. The dimers are stable during our observations. All dimers are made of identical particles (either two small particles or two large particles), indicating that they are formed prior to the experiment; they seem to be present in the samples as received. Rather than being two spheres barely touching, they are somewhat fused together, as can be seen in Fig. 2(a). The aspect ratio (length/width) is always less than two and varies from dimer to dimer.

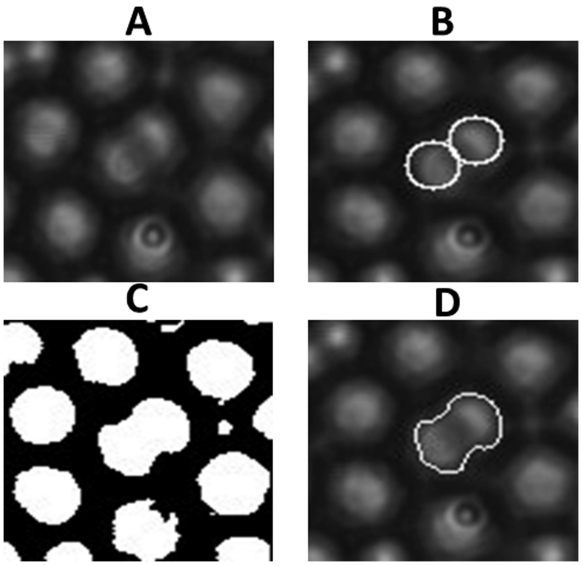

FIG. 2. (a) Image of a dimer surrounded by spherical particles. (b) Identification of two individual particles in a dimer. (c) Thresholded image. (d) Outline of the dimer from the thresholded image. The aspect ratio of the dimer is 1.65, and the size of the image is ~10 μm.

B. Imaging and tracking dimers

We need to follow the translational and rotational motion of the dimers. We start by using the standard particle tracking software[20] to track the two particles of a dimer, as shown in Fig. 2(b). Next we select the region of the image (ROI) that included dimers. Based on brightness, we threshold this ROI to get a black and white image [Fig. 2(c)]. We identify connected regions in this thresholded image and selected the largest such region as the dimer of interest. The length of the longest axis of this connected region is measured as l_l, and then we identify the length of the shortest axis l_s as the longest distance across the connected region perpendicular to the long axis. The aspect ratio then is l_l/l_s.

Recent work has shown that two-dimensional glass-forming systems need to be analyzed slightly differently than 3D systems.[19,21,22] The key concern is that 2D systems are subject to Mermin-Wagner fluctuations that move particles locally but do not lead to structural rearrangements.[22–27] Particles are "caged" by their neighbors, but Mermin-Wagner fluctuations result in coherent motion of the cage. Analyzing the motion of particles relative to their caging neighbors removes the influence of these fluctuations, making apparent the motions that lead to structural relaxation.[28]

Accordingly, to determine the relaxation time scale for our samples, we define the cage-relative translational correlation function as $F_{S-CR}(k, \Delta t) = \langle \exp(i\vec{k} \cdot \Delta\vec{r}_{CR}) \rangle_t$, where $\Delta\vec{r}_{CR} = \vec{r}(t + \Delta t) - \vec{r}(t) - \frac{1}{N}\sum_j [\vec{r}_j(t + \Delta t) - \vec{r}_j(t)]$, where j denotes the nearest neighbors of the particle at the initial time t, and the sum is over all neighbors. The α relaxation time scale τ_α is the time scale when F_{S-CR} reaches $1/e = 0.37$ and defines the time scale over which the sample has significant structural rearrangements.[19]

The cage-relative mean square displacement (MSD) is defined using the same displacements $\Delta\vec{r}_{CR}$. We measure the long time translational diffusion coefficient D_T from the cage-relative MSD. For our tracers, we do not see a significant difference between the MSD and the cage-relative MSD in the observed area fraction range. However, softer samples are known to have larger differences.[19,22] We are interested in the $\Delta t \to \infty$ behavior, so distinctions between motion along the dimer axis and perpendicular to that axis will not be important to us.[29] Rotational mean square displacements ($\mathrm{MSD_R}$) do not require cage-relative analysis. For $\mathrm{MSD_R}$, we identify the instantaneous angle $\theta(t)$ of a dimer (in radians), unwrap this angle so that it can take values smaller than 0 or larger than 2π; and then compute $\mathrm{MSD_R}$ from this unwrapped angle.

C. Hydrodynamic theory

The dimers we analyze have an aspect ratio $l_l/l_s < 2$, whereas perfect dumbbells have aspect ratio 2. Nonetheless, a reasonable starting approximation is to model our dimers as dumbbells. For dumbbells in a liquid, the ratio of translational to rotational diffusion coefficients is given as[30]

$$\frac{D_T}{D_R} = \frac{\sigma^2}{4}, \tag{1}$$

where σ is the diameter of particles in the dumbbell. This predicts a ratio of 1.60 $\mu\mathrm{m}^2/\mathrm{rad}^2$ for a dimer composed of

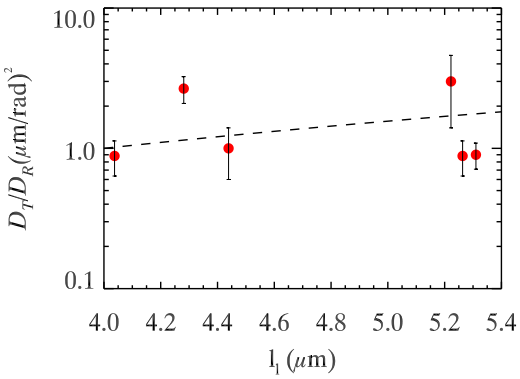

FIG. 3. D_T/D_R as a function of the dimer length l_l, from a medium-concentration sample with $\phi = 0.55$ ($\tau_\alpha = 9.5$ s). The dashed line is Eq. (1) using $\sigma = l_l/2$. Note that for these data, we are at low area fraction and so we use the normal MSD rather than the cage-relative MSD to measure translational diffusion constants.

two small particles in our experiment and 2.86 $\mu m^2/rad^2$ for a dimer composed of two large particles.

Figure 3 shows D_T/D_R as a function of dimer length l_l in a medium-concentration sample. The data are scattered with no systematic dependence on l_l. The dashed line shows Eq. (1), and the data are within a factor of two of this prediction. This is reasonable as (1) our dimers are not of a perfect dumbbell shape as assumed by theory and (2) Eq. (1) does not take into account the hydrodynamic influence of the bottom wall,[31] which affects translational and rotational modes differently.[29,32] It is also possible that the different values of l_l for dimers ostensibly made from identical particles give rise to dimers of different shapes (different amounts of overlap of the two particles), which could account for the scatter in our data. In sum, we recognize an inherent uncertainty for the ratio of D_T/D_R of about a factor of 2 and will look for this ratio to vary by more than a factor of two as we approach the glass transition.

III. RESULTS

Figure 4 shows translational and rotational MSDs in medium-concentration [(a) and (b)] and high concentration [(c) and (d)] samples corresponding to different length dimers. For the medium-concentration samples ($\phi = 0.55$), all MSDs rise diffusively, MSD $\sim \Delta t$, as can be seen by comparing the data to the straight black line which has slope = 1. The long dimer diffuses a bit slower, as seen by the blue diamonds lying below the red circles in Figs. 4(a) and 4(b). Interestingly at a large concentration ($\phi = 0.79$), we see that the translational MSD is similar for the short and long dimers [Fig. 4(c)], while the rotational MSD is much different [Fig. 4(d)]. Comparing Figs. 4(a) and 4(c), we see that both long and short dimers show a similar slow down in translation. However, Figs. 4(b) and 4(d) are very different. Here, long dimers (blue diamonds in this graph) show a much larger slowdown in rotation as compared with short dimers (red circles) at a high concentration.

Figure 5 shows the trajectories of the dimers corresponding to Fig. 4. For the medium-concentration sample (a), long and short dimers have similar trajectories. In contrast, the concentrated sample (c) shows that the long dimer

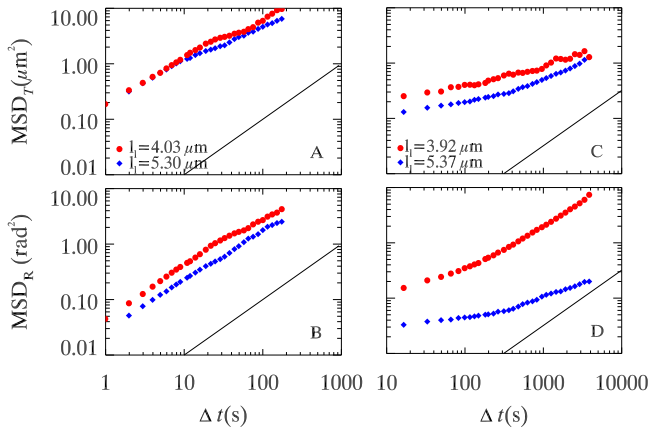

FIG. 4. (a) Cage-relative translational MSD of short ($l_l = 4.03$ μm, aspect ratio = 1.76) and long ($l_l = 5.30$ μm, aspect ratio = 2.00) dimers in a slightly supercooled sample at $\phi = 0.55$. $D_T = 0.015$ $\mu m^2/s$ and 0.009 $\mu m^2/s$ for the short and long dimers, respectively. (b) Rotational MSD of the same dimers as in (a). $D_R = 0.017$ 1/s and 0.01 1/s for the short and long dimers, respectively. (c) Cage-relative translational MSD of short ($l_l = 3.92$ μm, aspect ratio = 1.96) and long ($l_l = 5.37$ μm, aspect ratio = 1.80) dimers in a concentrated sample at $\phi = 0.79$. $D_T = 0.0015$ $\mu m^2/s$ and 0.000 08 $\mu m^2/s$ for the short and long dimers, respectively. (d) Rotational MSD of the same dimers as in (c). $D_R = 0.001$ 1/s and 0.000 03 1/s for the short and long dimers, respectively. In all panels, the black lines indicate a slope of 1, which is the case for diffusive behavior.

(blue) spends more time localized (perhaps with a reversible cage rearrangement event in the middle[33] and an irreversible jump at the end). The shorter dimer (red) moves more frequently.

Additionally, we track the angular motion of each dimer, shown in Figs. 5(b) and 5(d). This is easy to measure as we can track both particles in the dimer and hence compute the instantaneous angle θ. We keep track of the number of rotations so that θ is unbounded. In the medium-concentration sample, shown in Fig. 5(b), long and short dimers have similar angular

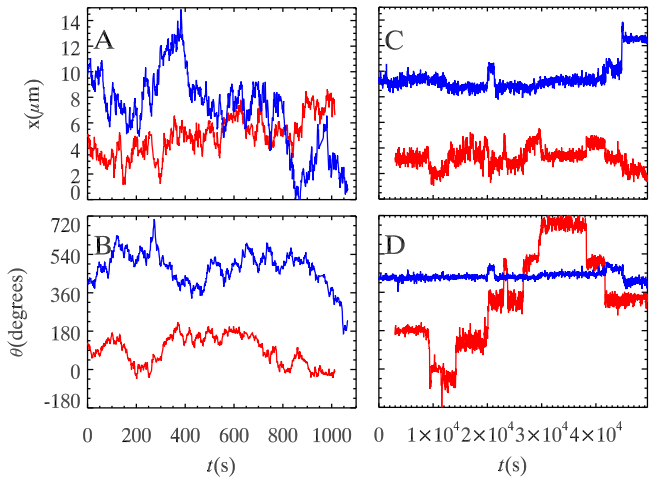

FIG. 5. (a) Cage-relative displacements in the x direction of short ($l_l = 4.03$ μm in red) and long ($l_l = 5.30$ μm in blue) dimers in a slightly supercooled sample at $\phi = 0.55$. These are the dimers analyzed in Figs. 4(a) and 4(b). (b) Angular trajectories corresponding to (a). (c) Cage-relative displacements in x of short ($l_l = 3.92$ μm in red) and long ($l_l = 5.37$ μm in blue) dimers in a concentrated sample at $\phi = 0.79$. These are the dimers analyzed in Figs. 4(c) and 4(d). (d) Angular trajectories corresponding to (c). Note that all trajectories are shifted to put each dimer onto the same graph; they are not actually adjacent dimers.

displacements. However in the concentrated sample shown in Fig. 5(d), clearly the short dimer (red) shows much larger angular displacements than the long dimer (blue). Thus the small dimer is able to rotate much easier than the long dimer. In particular, it often rotates by 180°, suggesting that the cage of neighboring particles expands slightly, the dimer has a chance to rotate, and then the cage contracts locking the dimer into the original orientation or else 180° rotated.

The short dimer shows jumps in angle at certain times. Figure 6 shows this dimer at three consecutive time points (a), (b), and (c) during which a large jump takes place. The time between each is the recording rate of 16.5 s/image (used for the concentrated sample). (d) shows this characteristic jump zoomed in. Clearly, the dimer rotates fairly quickly. While it is possible we miss rotations that are more than 180° between video frames, we believe this is unlikely. We examine the probability distributions of angular jumps between video frames, $P(|\Delta\theta|)$, and find that the probability of large jumps is nearly zero for $|\Delta\theta| > 170°$. This suggests that larger jumps with $|\Delta\theta| > 180°$ are even rarer.

To compare all our data, we fit the large Δt behavior of all MSD curves to measure diffusion constants. The translation diffusion coefficient D_T is measured as $\langle \Delta r^2_{CR}(\Delta t)\rangle = 4D_T\Delta t$ (using cage-relative displacements). The average is over all particles and all initial times. The rotational diffusion coefficients are measured similarly, through $\langle \Delta\theta^2(\Delta t)\rangle = 2D_R\Delta t$, where $\Delta\theta$ is the angular displacement in Δt. Figure 7(a) plots D_T as a function of τ_α (defined in Sec. II) for all samples. Here we see that all dimers follow the black line, which is the measured bulk D_T of the spherical particles in the sample. A fit to the bulk data (not shown) finds $D_T \sim \tau_\alpha^{-0.73}$, which is in the range of exponents observed in other experiments.[12,34]

Rotational diffusion also slows for glassy samples as shown by the data for D_R in Fig. 7(b). In contrast with D_T, these data become more scattered for the samples closer to the glass transition (larger τ_α). It is apparent that the slowest

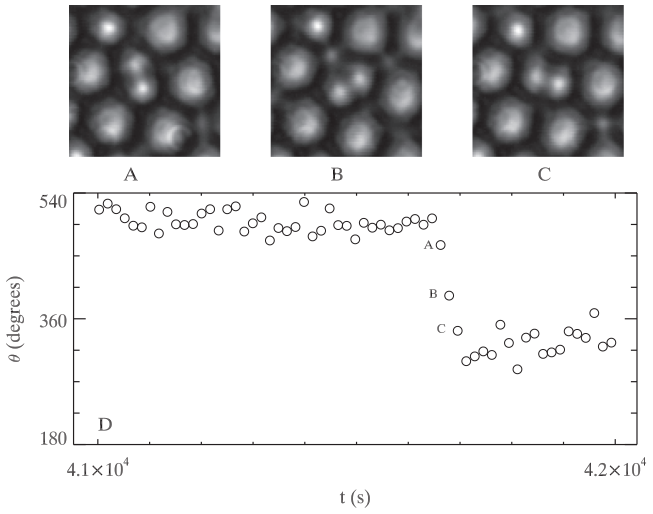

FIG. 6. Angular displacements of the short dimer, the same as shown in Fig. 5(d). Images show the corresponding dimer during certain short time interval, from (a) to (c). The size of each image is ~10 μm. (d) shows the zoomed-in interval of the large angular displacement, where *A*, *B*, and *C* are the same time points as the respective images.

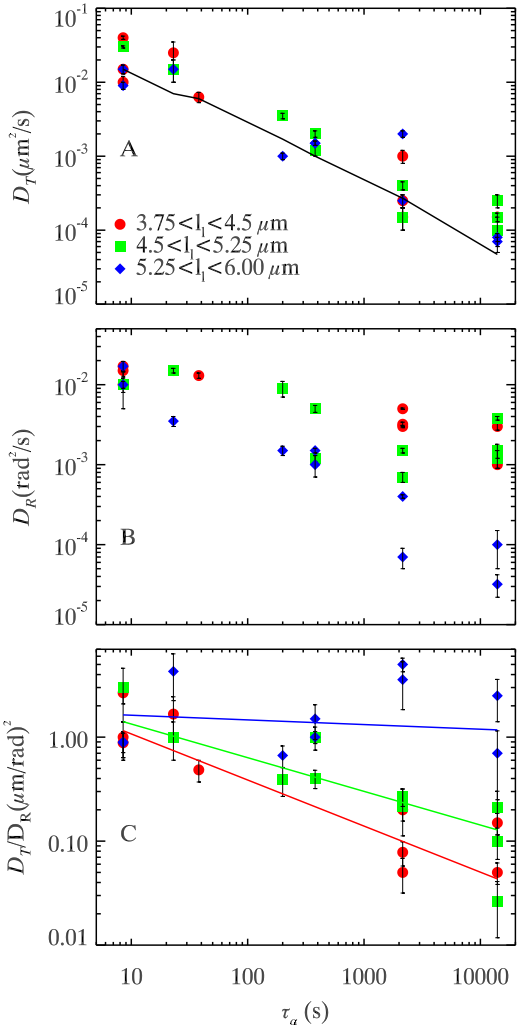

FIG. 7. Diffusion coefficients as a function of τ_α for different dimer lengths. (a) Translational diffusion constants D_T. The black line denotes the measured bulk sample D_T, that is, the diffusion coefficient of the spherical bath particles. (b) Rotational diffusion constants D_R. (c) The ratio D_T/D_R. In all the panels, the different colors denote different ranges of l_l as indicated in the legend in (a). The lines in (c) are power-law fits.

rotational diffusion is seen for the long dimers (blue diamonds) which slow by ~10^2–10^3 as τ_α grows by 10^3. In contrast, the short dimers (red circles) decrease by only ~10^1 over the same range. The difference between D_R of the long and short dimers is more than an order of magnitude at the largest τ_α. The mild decrease in D_R for the short dimers is similar to that seen with spherical colloids in a prior experiment.[13] Overall, this is what we expect based on the conceptual sketch of Fig. 1: long dimers require their neighbors to move out of the way to facilitate their rotation, whereas short dimers are constrained less by their neighbors. Likewise this is supported by Fig. 5(d) where the short dimer makes large jumps in angle.

We examine decoupling of rotational and translational diffusion by plotting D_T/D_R in Fig. 7(c). The long dimers (blue diamonds) show a constant D_T/D_R independent of τ_α; here the two diffusion constants are coupled at all area fractions. In contrast, the short dimers (red circles) show a decrease in D_T/D_R with increasing τ_α. The colored lines show power-law fits for the three different dimer length regimes. Some

of the observed spread in data could be due to dynamical heterogeneity. Closer to the glass transition, dynamical heterogeneity causes differences in diffusivities across the sample.[35] This could cause different particles of similar shape to differ in D_T/D_R depending on their local environment. However, at the largest τ_α, the difference between D_T/D_R of the long and short dimers is more than an order of magnitude. We see decoupling: while both rotational and translational diffusion slow as the glass transition is approached, rotational diffusion slows less dramatically—at least for the short dimers.

Organizing the data based on dimer length shows a clear trend from long dimers (no decoupling) to short dimers (decoupling); another possible variable is the aspect ratio. Figure 8(a) shows D_T/D_R plotted as a function of τ_α, equivalent to Fig. 7(c), but here different colors denote the aspect ratio instead of the dimer length. There is no clear trend with the aspect ratio, in strong contrast to Fig. 7(c). Hence the longest axis seems to be the relevant parameter, rather than the aspect ratio. A final way to think about the data is motivated by Fig. 5(d), showing that the short dimers can rotate by 180°; this is presumably because their cage of neighboring particles expands slightly, allowing the rotation. The expansion distance can be estimated as $l_l - l_s$, arguing that the neighbors start $\sim l_s$ away from the middle of the dimer and expand to $\sim l_l$ to allow the long axis to rotate past them. This suggests that the l_l dependence [Fig. 7(c)] could be a dependence on $l_l - l_s$. This seems plausible; Fig. 8(b) shows the data with colors indicating different ranges of $l_l - l_s$, which reasonably well separates the faster rotating dimers (red circles, small $l_l - l_s$) from the slower rotating dimers (green squares, large $l_l - l_s$). The fact that l_l works slightly better [Fig. 7(c)] may be because the number of neighbors that need to move scales as l_l, independent of l_s. Note that the slight cage expansion allowing the 180° rotation is likely unrelated to dynamical heterogeneity. While the cage expansions are uncommon events, the fluctuations in the cage size occur on a short time scale that is not directly related to long-time-scale rearrangement motions.[35]

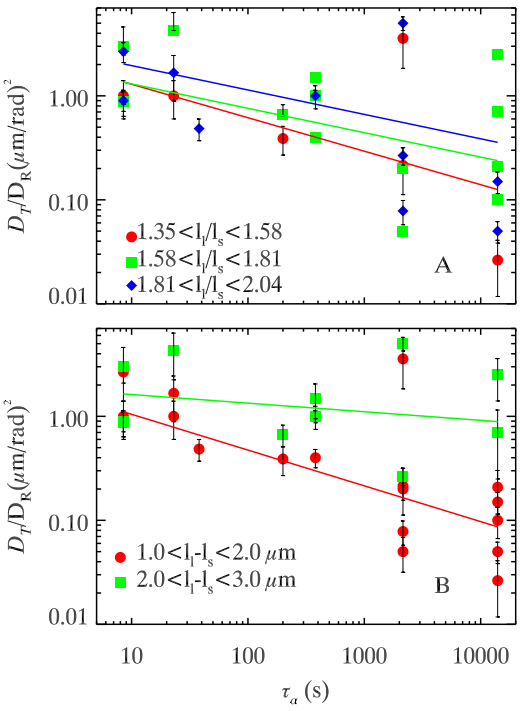

FIG. 8. (a) D_T/D_R as a function of τ_α for different aspect ratios l_l/l_s as indicated in the legend. (b) The same data for different values of $l_l - l_s$ as indicated in the legend. In both the panels, the lines are fits to the data.

Previous simulations found that quantifying translation-rotation decoupling depends on the analysis method.[12,36] The "Debye method" uses dot products of the initial and final orientation of a tracer; using this method to measure D_R changed the nature of decoupling.[12,36] We also measured D_R from this formalism, in the same way as done by Edmond *et al.*[14] We find that both methods to measure D_R give the same result within error, as also found by Edmond *et al.*

Our results indicate that the longest dimension controls how the particle rotation is sterically constrained by the neighbors on approaching the glass transition. Figure 1 suggests that this may be because the longest dimension determines how many neighboring particles can restrict rotational motion. Of course, all of our results are for a particular colloidal sample with particles having a size ratio 1:1.34. It is possible that the results would differ in other samples. With a larger size ratio, cages surrounding dimer tracers would vary strongly in composition, which might change the frequency of the fluctuations that allow 180° rotations such as Fig. 6.[37]

IV. DISCUSSION

Prior groups have studied glass transitions in colloidal glasses composed of anisotropic particles.[13,15,16] Kim *et al.*[13] studied rotation and translation of optically anisotropic spheres (aspect ratio 1). Here, D_T/D_R in the concentrated regime was almost 2 orders of magnitude smaller than the dilute limit.[13] As spheres rotate without any steric hindrance from neighboring spheres, in this experiment, translation slows down more than rotation approaching the glass transition.[13,18] More precisely, translation slows down dramatically, but rotation only slows slightly.

Other experiments by Zheng *et al.* looked at ellipsoids of aspect ratios varying from 2.3 to 6.[15,16] For the small aspect ratio of 2.3, D_T/D_R did not change approaching the glass transition, similar to what we see with our long dimers. For the large aspect ratio 6, however, D_T/D_R was an order of magnitude higher than the dilute limit, indicating that rotation slows down more than translation. This study concluded that the decoupling with enhanced translational motion occurs for situations with aspect ratio $\gtrsim 2.5$.[16] A similar observation of enhanced diffusion was seen by Edmond *et al.* who studied tetrahedral cluster tracers in a 3D sample of spherical particles.[14] There, the ratio between the longest dimension of the cluster to the mean particle size was 2.9. While a direct comparison between 2D ellipsoids and 3D tetrahedra seems dubious, nonetheless, the observations of Edmond *et al.*[14] are in conceptual agreement with the observation of Zheng *et al.*[16]

Our dimer experiments bridge the gap between aspect ratio ~1.3–2. We see that close to the glass transition, small changes in dimer length cause significant changes in rotational

diffusion. Smaller dimers show a weaker slowdown in rotation on approaching the glass transition. This is because smaller dimers rotate more freely even in a dense sample. Figure 5(d) shows that this easier rotation is likely due to slight motions of neighboring particles which momentarily allow a rotation of 180° for the short dimers. The results of Kim *et al.*[13] with spheres are the logical limit of our results, where a particle can rotate freely with only hydrodynamic interactions with neighbors but no steric hindrance to rotation. Summarizing all of the experimental observations from short to long particle shape, there are spheres that rotate easily,[13] short dimers that can make rapid jumps (Fig. 6), longer dimers with coupled translational and rotational diffusion [blue diamonds of Fig. 7(c)],[15,16] and still longer particles for which rotations are strongly inhibited and slower than translational motion.[14–16] Increasing the particle length relative to the cage size changes from decoupled fast rotation to coupled translation/rotation and to decoupled slow rotation. Of course, length is only one aspect of particle anisotropy;[38] our results suggest that steric hindrance from the cage surrounding a tracer is a useful idea which may inform coupling or decoupling of more complex particles.

In our experiments, translational diffusion is not affected as much by the dimer length. This is in marked contrast to previous experiments in polymer glasses, where translational diffusion was found to be affected by tracer shape and not rotational diffusion;[39] in polymer experiments, translational diffusion slowed down more than rotational diffusion as the glass transition was approached. These results are different from what we see, but more like the long ellipsoid experiments.[15,16]

In summary, our results bridge the prior colloidal observations, and collectively these observations show that steric interactions affecting rotational diffusion depend in an important way on the longest dimension of the tracer particles. This highlights the importance of steric interactions for understanding decoupling of translational and rotational diffusion near the glass transition.

ACKNOWLEDGMENTS

We thank J. C. Crocker for helpful discussions. This work was supported by the National Science Foundation (Nos. CMMI-1250235 for S.V. and DMR-1609763 for E.R.W.).

[1] G. Biroli and J. P. Garrahan, "Perspective: The glass transition," J. Chem. Phys. **138**, 12A301 (2013).
[2] M. D. Ediger and P. Harrowell, "Perspective: Supercooled liquids and glasses," J. Chem. Phys. **137**, 080901 (2012).
[3] A. Cavagna, "Supercooled liquids for pedestrians," Phys. Rep. **476**, 51–124 (2009).
[4] A. Einstein, "Über die von der molekularkinetischen Theorie der Wärme geforderte Bewegung von in ruhenden Flüssigkeiten suspendierten Teilchen," Ann. Phys. **322**, 549–560 (1905).
[5] W. Sutherland, "A dynamical theory of diffusion for non-electrolytes and the molecular mass of albumin," Philos. Mag. Ser. 6 **9**, 781–785 (1905).
[6] F. Fujara, B. Geil, H. Sillescu, and G. Fleischer, "Translational and rotational diffusion in supercooled orthoterphenyl close to the glass transition," Z. Phys. B: Condens. Matter **88**, 195–204 (1992).
[7] I. Chang, F. Fujara, B. Geil, G. Heuberger, T. Mangel, and H. Sillescu, "Translational and rotational molecular motion in supercooled liquids studied by NMR and forced Rayleigh scattering," J. Non-Cryst. Solids **172**, 248–255 (1994).
[8] L. Berthier, D. Chandler, and J. P. Garrahan, "Length scale for the onset of Fickian diffusion in supercooled liquids," Europhys. Lett. **69**, 320 (2004).
[9] S. K. Kumar, G. Szamel, and J. F. Douglas, "Nature of the breakdown in the Stokes-Einstein relationship in a hard sphere fluid," J. Chem. Phys. **124**, 214501 (2006).
[10] M. D. Ediger, "Spatially heterogeneous dynamics in supercooled liquids," Annu. Rev. Phys. Chem. **51**, 99–128 (2000).
[11] S.-H. Chong, A. J. Moreno, F. Sciortino, and W. Kob, "Evidence for the weak steric hindrance scenario in the supercooled-state reorientational dynamics," Phys. Rev. Lett. **94**, 215701 (2005).
[12] S.-H. Chong and W. Kob, "Coupling and decoupling between translational and rotational dynamics in a supercooled molecular liquid," Phys. Rev. Lett. **102**, 025702 (2009).
[13] M. Kim, S. M. Anthony, S. C. Bae, and S. Granick, "Colloidal rotation near the colloidal glass transition," J. Chem. Phys. **135**, 054905 (2011).
[14] K. V. Edmond, M. T. Elsesser, G. L. Hunter, D. J. Pine, and E. R. Weeks, "Decoupling of rotational and translational diffusion in supercooled colloidal fluids," Proc. Natl. Acad. Sci. U. S. A. **109**, 17891–17896 (2012).
[15] Z. Zheng, F. Wang, and Y. Han, "Glass transitions in quasi-two-dimensional suspensions of colloidal ellipsoids," Phys. Rev. Lett. **107**, 065702 (2011).
[16] Z. Zheng, R. Ni, F. Wang, M. Dijkstra, Y. Wang, and Y. Han, "Structural signatures of dynamic heterogeneities in monolayers of colloidal ellipsoids," Nat. Commun. **5**, 3829 (2014).
[17] P. N. Pusey and W. van Megen, "Phase behaviour of concentrated suspensions of nearly hard colloidal spheres," Nature **320**, 340–342 (1986).
[18] E. R. Weeks, "Introduction to the colloidal glass transition," ACS Macro Lett. **6**, 27–34 (2017).
[19] S. Vivek, C. P. Kelleher, P. M. Chaikin, and E. R. Weeks, "Long-wavelength fluctuations and the glass transition in two dimensions and three dimensions," Proc. Natl. Acad. Sci. U. S. A. **114**, 1850–1855 (2017).
[20] J. C. Crocker and D. G. Grier, "Methods of digital video microscopy for colloidal studies," J. Colloid Interface Sci. **179**, 298–310 (1996).
[21] H. Shiba, Y. Yamada, T. Kawasaki, and K. Kim, "Unveiling dimensionality dependence of glassy dynamics: 2D infinite fluctuation eclipses inherent structural relaxation," Phys. Rev. Lett. **117**, 245701 (2016).
[22] B. Illing, S. Fritschi, H. Kaiser, C. L. Klix, G. Maret, and P. Keim, "Mermin–Wagner fluctuations in 2D amorphous solids," Proc. Natl. Acad. Sci. U. S. A. **114**, 1856–1861 (2017).
[23] R. Peierls, "Bemerkungen über umwandlungstemperaturen," Helv. Phys. Acta **7**, 81–83 (1934).
[24] L. D. Landau, "Zur theorie der phasenumwandlungen II," Phys. Z. Sowjetunion **11**, 26–35 (1937).
[25] N. D. Mermin and H. Wagner, "Absence of ferromagnetism or antiferromagnetism in one- or two-dimensional isotropic Heisenberg models," Phys. Rev. Lett. **17**, 1133–1136 (1966).
[26] N. D. Mermin, "Crystalline order in two dimensions," Phys. Rev. **176**, 250–254 (1968).
[27] C. L. Klix, G. Maret, and P. Keim, "Discontinuous shear modulus determines the glass transition temperature," Phys. Rev. X **5**, 041033 (2015).
[28] S. Mazoyer, F. Ebert, G. Maret, and P. Keim, "Dynamics of particles and cages in an experimental 2D glass former," Europhys. Lett. **88**, 66004 (2009).
[29] Y. Han, A. M. Alsayed, M. Nobili, J. Zhang, T. C. Lubensky, and A. G. Yodh, "Brownian motion of an ellipsoid," Science **314**, 626–630 (2006).
[30] L. F. Cugliandolo, G. Gonnella, and A. Suma, "Rotational and translational diffusion in an interacting active dumbbell system," Phys. Rev. E **91**, 062124 (2015).
[31] E. Sarmiento-Gómez, J. R. Villanueva-Valencia, S. Herrera-Velarde, J. A. Ruiz-Santoyo, J. Santana-Solano, J. L. Arauz-Lara, and R. Castañeda Priego, "Short-time dynamics of monomers and dimers in quasi-two-dimensional colloidal mixtures," Phys. Rev. E **94**, 012608 (2016).
[32] S. Bhattacharya, J. Blawzdziewicz, and E. Wajnryb, "Hydrodynamic interactions of spherical particles in suspensions confined between two planar walls," J. Fluid Mech. **541**, 263–292 (2005).
[33] K. Vollmayr-Lee, "Single particle jumps in a binary Lennard-Jones system below the glass transition," J. Chem. Phys. **121**, 4781–4794 (2004).
[34] M. G. Mazza, N. Giovambattista, H. E. Stanley, and F. W. Starr, "Connection of translational and rotational dynamical heterogeneities with the breakdown of the Stokes-Einstein and Stokes-Einstein-Debye relations in water," Phys. Rev. E **76**, 031203 (2007).

[35]E. R. Weeks, J. C. Crocker, A. C. Levitt, A. Schofield, and D. A. Weitz, "Three-dimensional direct imaging of structural relaxation near the colloidal glass transition," Science **287**, 627–631 (2000).
[36]T. G. Lombardo, P. G. Debenedetti, and F. H. Stillinger, "Computational probes of molecular motion in the Lewis-Wahnström model for ortho-terphenyl," J. Chem. Phys. **125**, 174507 (2006).
[37]R. Kurita and E. R. Weeks, "Glass transition of two-dimensional binary soft-disk mixtures with large size ratios," Phys. Rev. E **82**, 041402 (2010).
[38]S. C. Glotzer and M. J. Solomon, "Anisotropy of building blocks and their assembly into complex structures," Nat. Mater. **6**, 557–562 (2007).
[39]D. B. Hall, D. D. Deppe, K. E. Hamilton, A. Dhinojwala, and J. M. Torkelson, "Probe translational and rotational diffusion in polymers near Tg: Roles of probe size, shape, and secondary bonding in deviations from Debye–Stokes–Einstein scaling," J. Non-Cryst. Solids **235-237**, 48–56 (1998).